Geoderma 153 (2009) 269–277

Contents lists available at ScienceDirect

Geoderma

journal homepage: www.elsevier.com/locate/geoderma

Measuring physical and hydraulic properties of peat from X-ray tomography

W.L. Quinton [a,*], T. Elliot [b], J.S. Price [c], F. Rezanezhad [a], R. Heck [b]

[a] Cold Regions Research Centre, Wilfrid Laurier University, Waterloo, Canada N2L 3C5
[b] Department of Land Resource Science, University of Guelph, Guelph, Canada N1G 2W1
[c] Department of Geography, University of Waterloo, Waterloo, Canada N2L 3G1

ARTICLE INFO

Article history:
Received 29 February 2008
Received in revised form 25 February 2009
Accepted 17 August 2009
Available online 13 September 2009

Keywords:
Peat
X-ray tomography
Moisture content
Active porosity
Physical properties
Hydraulic properties

ABSTRACT

Organic soils cover a large percentage of the Canadian land mass in the form of peatlands (14%) and other organic terrains, including arctic and alpine tundra and taiga (25%). *Sphagnum* mosses are the dominant peat-forming species in all of these terrains. Understanding the processes by which this material conducts, retains and redistributes moisture and energy is crucial to the successful development of physically-based methods of measuring and modelling their hydrological response. *Sphagnum*-peat was sampled from Scotty Creek, in the wetland-dominated zone of discontinuous permafrost near Fort Simpson, Northwest Territories, Canada. Physical properties of the peat samples were measured from standard methods, and X-ray tomographic images of sub-samples were obtained at 5 levels of volumetric moisture content between ~0.4 and 0.7. The volumetric moisture content measured using the tomographic images closely approximated the gravimetric measurements. Properties of the pore spaces were measured in both two and three dimensions. The active porosities measured in 2D and 3D were very similar, and matched closely with values reported in the literature. Specific surface area (3D), however, was larger than the specific perimeter (2D). The 2D analysis suggests a relatively gradual transition from small to large pores; while in 3D, the distribution is dominated by a single large pore space, whose volume and surface area are 3-orders of magnitude larger than the next largest pore, and >99% of the total inter-particle pore volume. This single, large pore space contains the flow network. This study elucidated the volume and configuration of this network for discrete ranges of soil water pressure that typically occur in the field. The flow network diminished from 17.6% to 9.0% of a sample volume as its volumetric moisture content lowered from 0.65 to 0.42. This volume loss was accommodated by the thinning and disaggregation of moisture films, although as the sample lost moisture, the flow network maintained a relatively even spatial distribution.

1. Introduction

Peat deposits cover large areas of northern North America and Eurasia, in the form of arctic and alpine tundra, taiga, boreal and sub-boreal bogs, fens and other peatlands, in which *Sphagnum* mosses are the dominant peat-forming species. As a result, there is a similarity among these site types with respect to the physical properties of their peat deposits (Quinton et al., 2000). While some basic hydraulic properties including total porosity, specific yield and bulk density are well documented (Boelter, 1976; Boelter and Verry, 1977; Ingram, 1978), the pore size, shape and distribution that govern these have not been well described, nor the implications of these properties on water retention and flow pathways. Knowledge of pore geometry will aid in our understanding of water and solute fluxes, water storage mechanisms and hydraulic parameterisation.

Peat decomposition increases with depth below the ground surface, resulting in a decrease in the diameter of soil pores (Quinton et al., 2000). The latter strongly controls the resistance to flow, as the hydraulic conductivity increases with the square of pore diameters (Freeze and Cherry, 1979). Field and laboratory measurements indicate that hydraulic conductivity decreases with depth by two to three orders of magnitude in the upper 30 cm of peat at a variety of northern organic terrains (Quinton et al., 2008). However, the key processes by which peat conducts, retains and redistributes moisture are poorly understood. This is in large part due to the lack of understanding of how water flows among the organic fragments through the highly inter-connected pore space, and how the nature of this flow changes with variations in soil moisture content. This inter-particle pore space is referred to by Hoag and Price (1997) as the 'active porosity', since it is the fraction of the total porosity that conducts water when the peat is saturated. The void space within the peat fragments, including the remains of plant cells and other dead-end spaces, does not normally conduct water and is therefore referred to as the inactive porosity (Hayward and Clymo, 1982; Hoag and Price 1997).

The first step toward understanding how water is conveyed through peat is to characterise the flow network — that part of the active porosity conducting water. When peat is saturated, the active porosity defines

* Corresponding author. Tel.: +1 519 884 0710x3281; fax: +1 519 725 1342.
E-mail address: wquinton@wlu.ca (W.L. Quinton).

0016-7061/$ – see front matter © 2009 Elsevier B.V. All rights reserved.
doi:10.1016/j.geoderma.2009.08.010

the flow network; however, as the peat drains, air is introduced and water flow is restricted to liquid films, whose thickness and interconnectivity decrease with increasing drainage. Laboratory analyses, using pressure plates to derive water retention characteristic curves on peat samples from Scotty Creek provide some insight into the active porosity and the flow network. For example, it was found that the peat from the upper, lightly decomposed fibric layer, as well as well humified peat sampled from greater depths, drains to a residual moisture value of about 20% per volume at low (*c.* −100 to −500 cm) soil water pressures (Quinton and Hayashi, 2007); indicating that the active porosity is smaller than the total porosity by ~20%. Field studies at Scotty Creek indicate that even during the winter months when the moisture content is close to the residual of 20% unfrozen moisture by volume, there is still appreciable moisture redistribution throughout the peat profile (Quinton and Hayashi, 2007).

The traditional method of microscopic analysis of mineral soils includes acetone replacement, resin-impregnation, followed by the preparation and analysis of soil thin sections (FitzPatrick, 1984; Hoag and Price, 1997). This has been met with mixed success when applied to peat, owing to shrinkage and the secretion of wax into the resin during the drying and hardening phases. At best, these problems can cause substantial delays in sample preparation, while in other cases, they render the samples unusable. Some of these issues can be avoided by forgoing the development of thin sections, and instead, imaging the impregnated blocks directly (*e.g.* Quinton et al., 2008). Images of such blocks are enhanced if the resin contains fluorescent dye and the images are acquired under UV light. However thin sections and blocks only provide a 2D perspective, thus an uncertain conceptualisation of the true 3D system. Moreover, as all moisture is removed during their development, neither sections nor blocks can show moisture films, and thus cannot elucidate the flow network.

The 2D image analysis of Quinton et al. (2008) showed that the geometry of peat pore spaces is so highly complex that some of the underlying assumptions present in many classical expressions of flow through porous media, such as the Hazen (1911) and Kozeny–Carman (Carrier, 2003) equations, must be called into question. For example these equations assume that pores are sufficiently close to being circular in cross-section, that a single empirical or theoretical coefficient can be used to correct for non-circularity and other geometric pore properties, with the exception of pore size which was generally inferred, from water retention characteristic curves for example. Detailed measurements of the peat pore space are therefore required in order to properly parameterise hydraulic properties of peat.

The availability of computer tomographic (CT) imaging (Salem and Chilingarian, 1999) provides a new opportunity to evaluate the 3D pore geometry and its role in defining fundamental hydraulic properties of peat. CT imaging has been applied to a variety of geological materials, although most applications involve mineral soils (Olsen and Borresen 1997) and rock (Nakashima and Kamiya, 2007), while application to peat is rare. This approach involves rotational X-ray imaging of peat samples, followed by reconstruction of the imaged samples in a 3D digital form. It is advantageous in that it dramatically reduces the time delay between the field sampling and laboratory analysis stages. It also produces a much larger sample size than can be captured on thin sections or blocks, without significantly compromising the image resolution. Since this approach is non-destructive, the same sample can be re-scanned for different moisture conditions. This method also offers the prospect of examining small-scale soil structures in 3D. Therefore, the objectives of this paper are to 1) evaluate the use of X-ray tomography as a means of examining the volumetric content and distribution of moisture in peat; 2) measure and compare selected physical properties using 2D and 3D images of a common set of peat samples; and 3) directly measure selected media properties that are known to affect the saturated and unsaturated hydraulic conductivities.

2. Study area and methodology

2.1. Procedure for field sampling of soil blocks

The peat samples for this study were taken from a peat plateau in the continental high boreal wetland region (NWWG, 1988) of Scotty Creek (61° 18′N; 121°, 18′W), in the zone of discontinuous permafrost on 16 June, 2006. At this site, the tree cover includes *Picea mariana*, *Pinus contorta* and *Betula papyrifera*. As with temperate peatlands and organic-covered permafrost terrains, *Sphagnum* mosses are the dominant peat-forming species on peat plateaus. The peat profile contained an upper layer of living and lightly decomposed vegetation and fibric peat, overlying a darker layer of peat in a more advanced state of decomposition. The focus of the analyses was upon the upper peat layer, since it is this layer that conducts most of the drainage during the spring freshet. The volumetric moisture content of the upper layer rarely falls below 35% during the summer months. Peat plateaus also have the same essential characteristics of subsurface drainage as other widely occurring, organic-covered permafrost terrains whereby during soil thawing, the relatively impermeable frost table moves downward through a peat profile in which the hydraulic conductivity decreases exponentially with depth (Quinton et al., 2000).

A peat block with a surface dimension of 40 × 40 cm was removed using a flexible saw to cut vertically downward from the ground surface to the frost table at 30 cm depth. This procedure separated the sample block from the surrounding peat on its four sides. A small pit was then excavated on one side of the sample block; and the saw was used to cut horizontally to separate the base of the sample from the underlying frozen, saturated peat. The peat block was then lifted and placed into an insulated container with the same internal dimensions. The predominantly *Sphagnum* vegetation living on the top of the peat block, was left intact. The sample container was refrigerated while transported to the Cold Regions Research Centre, Wilfrid Laurier University.

2.2. Peat sample preparation in laboratory

To minimise disturbance to the peat block during sub-sampling, the block was saturated with water while still in the container used for transport. The sample was saturated from the bottom, and the procedure took several hours as care was taken to minimise the formation of air bubbles. Once saturated, the sample and container were placed in a freezer at −10 °C for 48 h. The saturated, frozen peat block was then removed from the sample container, and three cylindrical sub-sample cores, each 10 cm long and 6 cm in diameter, were extracted from one side of the peat block using a hollow drill bit mounted on a drill press. The cores were sampled horizontally, with the upper, middle and lower cores representing the 0–6 cm, 6–12 cm and 12–18 cm depth ranges, all within the highly conductive, upper organic layer (Quinton et al., 2008). Each core was weighed and then inserted into a transparent, acrylic, 15 cm long, 6 cm inner-diameter tube and allowed to thaw and freely drain for 48 h. During this process, the samples were covered with a plastic sheet (*Parafilm*) to minimise evaporative loss of moisture. The samples remained in these tubes for all subsequent analyses. All calculations involving the soil volume (*i.e.* volumetric moisture content, bulk density, total porosity) were based on the thawed sample volume.

2.3. Measurement of peat properties

Selected physical properties of the three soils cores are summarised in Table 1. The total porosity of each sample core was computed from:

$$\phi_T = \frac{(W_{fs} - W_d)/V_s}{\rho_w} + f_b, \quad (1)$$

Table 1
Depth range (cm) of the horizontally-oriented core below the ground surface, total porosity ϕ_T, solid fraction $1-\phi_T$, bulk density ρ_b (kg m^{-3}), and ΔVol is the sample volume at −40 cm soil water pressure expressed as a percentage of the volume of the same sample at −2 cm soil water pressure (%).

Sample	Depth	ϕ_T	$1-\phi_T$	ρ_b	ΔVol (%)
Upper	0–6	0.955	0.044	35	88
Middle	6–12	0.863	0.137[a]	54	84
Lower	12–18	0.933	0.066	71	94

The sample volumes were 279.9 cm^3, 265.2 cm^3 and 271.4 cm^3 for the Upper, Middle and Lower cores respectively.
[a] Contained large woody roots.

where W_{fs} is the initial weight of the sample in the frozen, saturated state [g], W_d its dry weight measured following all analyses and after 48 h of drying at 105 °C [g], V_s is the volume of the sample in the unfrozen state before pressure was applied [cm^{-3}], and ρ_w is the density of water [g cm^{-3}]. The term f_b is the volume fraction of air bubbles in the sample in the frozen, saturated state; and was computed from:

$$f_b = f_a - \frac{(W_{fs} - W_{-2})/V_s}{\rho_w}, \quad (2)$$

where f_a is the volume fraction of air-filled voids measured on representative 3D tomographic images (see below) of each soil core using a reference soil water pressure of −2 cm, W_{-2} is the weight [g] of the soil at the reference pressure level, and the remaining terms are defined above. Although any of the five soil water pressures could have been used as the reference, we believe the error in estimating f_b from Eq. (2) is least when based on the moisture condition closest to saturation. The volume fraction of air bubbles computed from Eq. (2) was 0.125, 0.077, and 0.106 for the Upper, Middle and Lower samples, respectively.

Bulk density was measured gravimetrically following the method of Boelter (1976). Soil water pressure was measured using twin pressure plates constructed from a clear plexiglass 5.8 cm i.d. cylinder capped and sealed with 5.8 cm diameter disks at both ends. On each pressure plate one disk was perforated and had 25 μm Nitex fabric glued to it to provide an air entry pressure of about −40 cm, and the other disk was connected to an outflow hose. The twin pressure plates contacted the peat cores at both ends of the sample tubes, and the water pressure was set by lowering the hanging columns of water to −2, −10, −18, −30 and −40 cm soil water pressures, and at each pressure volumetric water content was measured gravimetrically (Price et al., in press). The sample volumes were also measured at each pressure level, and the measured values were used in the calculation of VMC so that the gravimetric calculation was based on the same sample volume imaged by the CT scanner.

2.4. X-ray CT imaging

Each sample was scanned at −2, −10, −18, −30 and −40 cm pressure levels, for a total of 15 scans. Upon reaching these pressure levels, the sample tubes were disconnected from the pressure plates and inserted into the X-ray CT scanner. A polyethylene sample marker, used to indicate direction and provide a registration datum, was inserted within the sample tube to facilitate co-registration of imagery produced. The scans were made using a GE Medical μCT, model MS8X-130, second generation cabinet scanner, and the samples were imaged at 100 kV 80 mA, 3500 ms exposure to obtain the optimal separation of the three phases of air, water, and organic material. A high pass filter was used to reduce hardening artifacts, and enhance contrast between sample phases. The series of rotational X-ray images was reconstructed to a 3D volume using a noise-reducing filtered back-projection algorithm. In order to reduce the presence of ring-artifacts in the 3D volume a de-speckle algorithm was run, which uses the median of a local kernel to identify signal noise as opposed to sample constituent variability. The imagery was acquired at a cubic-resolution of 16.7 μm for 64 mm diameter (bulk) samples. After tomographic reconstruction, the sample resolution was 45 mm. To reduce inherent noise and partial volume effects that are present in X-ray CT data, the authors employed a noise-reducing homomorphic filter and threshold determination technique which sub-samples the data based on neighbourhood homogeneity to provide better separation of peat constituent values (Elliot and Heck, 2007). After each scan, the sample tubes were reconnected to the twin pressure plates until the next pressure level was reached. The 2D and 3D analyses were conducted on the same 900×900×79 pixel volumes; although for the 2D analyses, each of the 79 slices were analysed separately. For 2D, only the *z*-positive surface was analysed, rendering each volume element (i.e. voxel) a pixel. Since the area of each 2D slice was 900×900 pixels, the stack of 79 slices had a volume of 5.8 cm^3.

2.5. Assessment of volumetric water content from CT images

Each voxel within the image was classified as either air or water/organic matter following the method of Elliot and Heck (2007). The grouping of water and organic matter was necessary since the latter is highly porous, and therefore when wet, attenuates in a manner very similar to water. For the purpose of this analysis, the volumetric linear attenuation coefficient (LAC) of organic matter was considered negligible at low soil water pressures (0 to −40 cm, or nearly-saturated samples) due to the partial volume effect. The partial volume effect results from subdivision of a 3D data matrix by a diagonal plane (such as the point of departure between two peat constituents), which creates a singular voxel containing two discrete materials. The resulting LAC is a compositional (volumetric) relationship of the two material LAC values.

2.6. Identifying the flow network

Through multiple imaging sessions, the segmented, or binary, imagery provided a numerical volumetric quantification of the two phases, indicating where and by how much the air intrusion/water evacuation occurred within the organic matter at various soil water pressure levels. To achieve a spatial measurement of change in moisture content and distribution with pressure, a co-registration of sample imagery was performed in 3D by the stack-alignment plug-in of ImageJ (Rasband, 2007). Following registration, regions of change were isolated (ΔV_{void} or $\Delta V_{non\text{-}void}$), through image subtraction wherein the voxels that differ in their classification between imagery data-sets are separated. The 3D ΔV_{void} or $\Delta V_{non\text{-}void}$ volumes were compared between pressure levels in order to map the 'active' flowpaths for the selected range in soil water pressures. The 5.8 cm^3 volume described above for the measurement of peat properties was found to be too narrow in the *z*-direction for this analysis. Instead, a 7.1 cm^3 volume with dimensions of 625×625×200 voxels was used. This larger volume was centred on the same voxel as the former.

3. Results and discussion

3.1. Volumetric moisture estimates from CT scans

X-ray attenuation varies throughout a sample owing to the variation in the mass densities of its constituents. The relative densities of sample constituents are expressed using the Hounsfield unit (HU) which assigns to each voxel an intensity value between −1500 and 1000, the former of which results from preferential attenuation of low energy X-rays emitted from the polychromatic source. Air space typically is assigned an HU of −1000, although it was found to be as low as −1500 in the sample imagery, whereas water retained a HU

of approximately 0. The large density difference between void voxels (i.e. air), and the remaining constituents of water and organic solids represented by the non-void voxels, results in a bi-modal distribution on a histogram of relative density for the peat samples (Fig. 1). The CT data contains 3D regions of homogeneous HU representing specific constituents separated by transition regions of highly-variable HU.

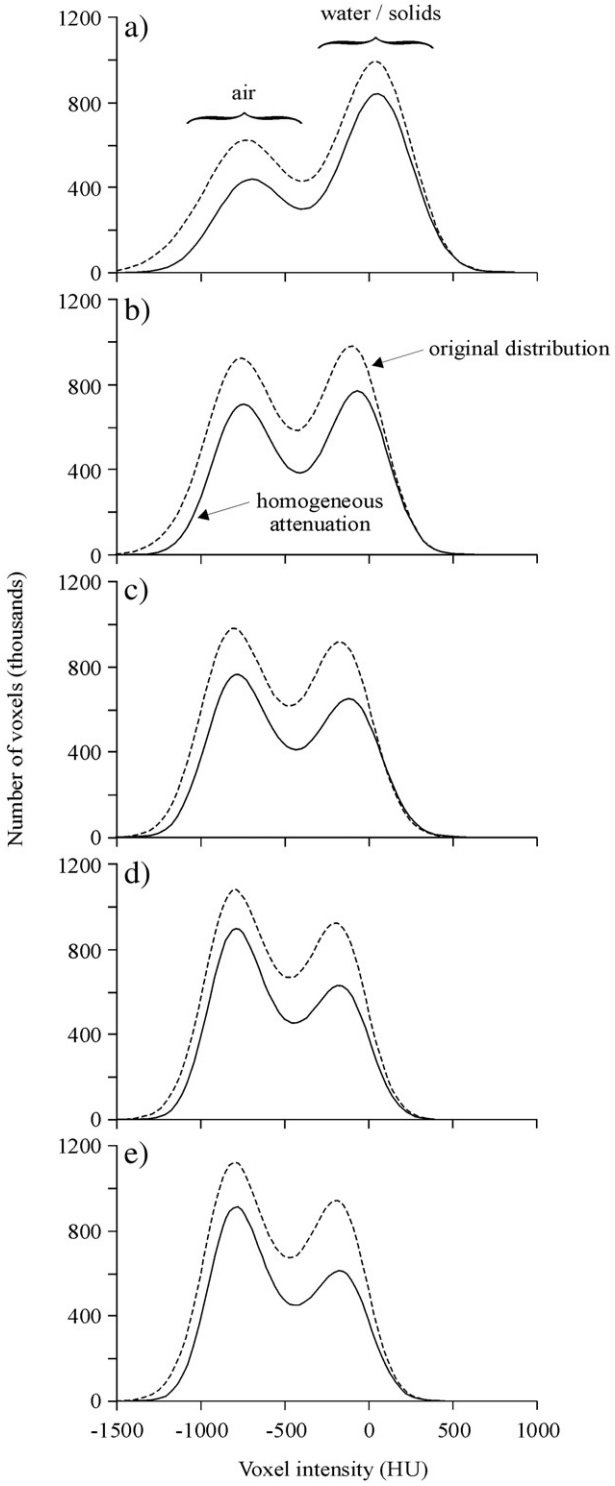

Fig. 1. Histograms of voxel intensity in Hounsfield units (HU) at five levels of soil water pressure applied to the Upper peat sample: −2 cm (a), −10 cm (b), −18 cm (c), −30 cm (d) and −40 cm (e). Original distribution of HU is shown as a dashed line for each soil level, and the HU of regions isolated based on homogeneous X-ray attenuation within a spatial neighbourhood, are indicated by the solid line.

Preferentially removing the transition regions (i.e. partial volumes) is desirable for the purpose of image classification (Elliot and Heck, 2007). By identifying regions of low HU variance, it can be assumed that the voxels within them are composed primarily of a single constituent. With this concept, separation of the original bi-modal peaks, shown as a dashed line in Fig. 1, within the histograms was further differentiated by specifically retaining regions of homogeneous linear attenuation coefficient (LAC), as per Elliot and Heck (2007), which form the solid-line histograms of Fig. 1. As soil water pressure decreased and water drained from the samples, the histogram was redistributed such that the area below the curve representing the void voxels, increased proportionately with a decrease in area below the curve representing the non-void voxels. Fig. 1 also shows some slight lateral shift of the histogram peaks among the pressure levels. For instance, in Fig. 1a, the reference densities of air and water had greater values than those for Fig. 1b. This is an artefact of the calibration procedure, which is performed individually for each scan.

In this study, the solid and liquid fractions of the histograms presented in Fig. 1 were not separated, as there is at present no effective algorithm to accomplish this for organic soils. Therefore, the non-void voxels represent the solid fraction, the water imbibed within it, and the water occupying the active porosity. The volumetric moisture content of soil core sub-samples computed from the fraction of non-void voxels (Fig. 2), therefore exceeded the gravimetric measurements of the soil cores, by an amount approximately equal to the fractional volume of solids, which for the three samples ranged between 0.044 and 0.137 (Table 1). As a result, the best-fit line in Fig. 2 is horizontally-displaced from the 1:1 line by an amount equal to the average solid fraction of the sub-samples analysed. However, since such a measure cannot be made directly on the sub-samples, the average solid fraction of the three sample cores of 0.083 (Table 1) serves to define the magnitude of displacement resulting from grouping water and the solid fraction into a single class. Assuming a slope of one, and setting the x-intercept to 0.083, a best-fit line is produced from linear regression that plots through the volume-adjusted data points ($R^2 = 0.83$) (Fig. 2). Fig. 2 also indicates the magnitude of error resulting from failure to account for drying-induced shrinkage of organic soils when computing their volumetric moisture content. The sample volume at −40 cm soil water pressure

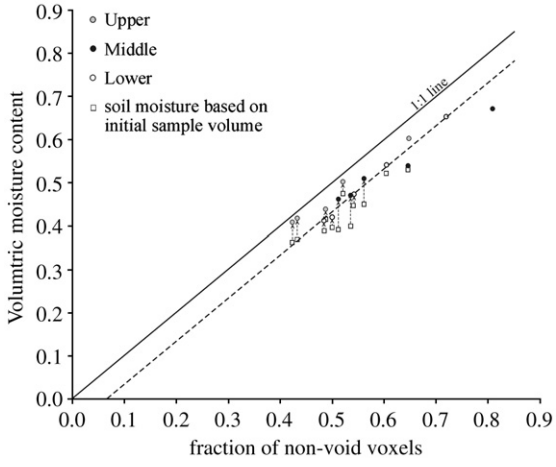

Fig. 2. Volumetric moisture content measured gravimetrically, plotted with that derived from the CT scan analysis. The data represents the three peat cores and five soil water pressure levels used in acquiring the CT images. The arrows indicate the degree to which the gravimetric soil moisture is altered when the calculation is based on the updated sample volume measured at each soil water pressure level. The initial volume refers to the sample volume measured at the soil water pressure of −2 cm: 279.9 cm^3, 265.2 cm^3 and 271.4 cm^3 for the Upper, Middle and Lower sample core, respectively. The moisture content derived from CT scan analysis was measured on 7.1 cm^3 (625×625×200 voxels) sub-samples within each sample core.

was as low as 84% of its value at −2 cm pressure (Table 1). The data presented in Fig. 2 and Table 1 suggests that X-ray tomography can be used to measure volumetric soil moisture of peat provided the fractional volume of solids is known. By extension, these findings also provide a reason to investigate the possibility that X-ray tomography can also be used to examine other physical properties of the void and non-void regions of peat samples.

3.2. Comparison of 2D and 3D analytical results

Active porosity was measured at the lowest pressure (−40 cm) since it was assumed that at this pressure, most of the inter-particle space would be air-filled and could therefore be distinguished from the rest of the media. For the 2D images, active porosity was computed from:

$$\phi_A = \sum_i A_i / A_{img}, \quad (3)$$

where A_i [L^2] is the area of the i-th pore on all seventy-nine 900×900 pixel slices. For all three samples, there was <5% variation among the seventy-nine computed values for ϕ_A (Table 2). The average active porosity $\bar{\phi}_A$, is within the range of values reported in the literature by studies that based their measurements on the analysis of thin sections (*e.g.* Hoag and Price, 1997; Quinton et al., 2000) and resin-impregnated soil blocks (*e.g.* Quinton et al., 2008). An active porosity of approximately 60% is reasonable given that the difference between it and the average measured total porosity of ~90% (Table 1), is accounted for by the sum of the inactive porosity, which is typically ~20% (*e.g.* Hoag and Price, 1997); and a residual of ~10% that would be accommodated by the water held in the remaining films at the −40 cm pressure. The measurements of active porosity based on imagery obtained at this pressure level are therefore underestimated by approximately 10%.

The decrease in active porosity with depth indicates an increased proportion of solids per unit volume of sample, which is a consequence of the collapse of the larger pores with depth due to decomposition (Hayward and Clymo 1982) and the weight of the overlying peat. This is evident from the increase in pore density (*i.e.* number of pores per cm^2) and decrease in pore size with depth (Table 2). The latter was calculated as the equivalent circular pore diameter (d_{cir}) by:

$$d_{cir} = 2\sqrt{\frac{\bar{A}}{\pi}}, \quad (4)$$

where ($\bar{A}$) is the mean pore area of each depth. The computed pore diameters (Table 2) were within 20% of the diameters reported by Quinton et al. (2000) for the same depth. Table 2 also indicates that the largest pore at each depth occupied a relatively small proportion (<2%) of the active porosity, suggesting that water in the flow network is not conveyed preferentially through a small number of large pores.

To estimate active porosity (ϕ_A) from the 3D data set, A_i and A_{img} in Eq. (3) were substituted with V_i and V_{img}, the volume of the i-th pore and the total image volume, respectively. The equivalent spherical pore diameter (d_{sph}) was calculated as:

$$d_{sph} = 2\left(\bar{V}\frac{3}{4\pi}\right)^{\frac{1}{3}}, \quad (5)$$

where $\bar{V}$ is the mean pore volume of each sample depth (Table 3). The active porosity measured in 3D (Table 3), produced essentially the same results as the 2D analysis (Table 2), demonstrating that a 2D measurement of ϕ_A yields an accurate estimate of this parameter for the 3D media. However, the equivalent pore diameters determined from the 2D analysis were 45%, 27% and 21% larger, respectively, for the 0–6, 6–12 and 12–18 cm depths, than calculated from the 3D images. The 3D results also indicated greater variation of pore density between the layers. For example, in 3D, the pore density (*i.e.* number of pores per cm^3) increased by about a factor of three between the middle and lower depth (Table 3), compared with a two-fold increase based on 2D analysis (Table 2).

The distributions of pore size derived from the 3D measurements are starkly different from those derived in 2D. The 2D view of peat indicates a more gradual transition from large to small pores; while in 3D, the distribution is dominated by a single large pore space, whose volume and surface area are 3-orders of magnitude larger than the next largest pore (Fig. 3). This single large pore is readily observed on the 2D and 3D images as the inter-connected pore space that extends throughout the peat sample (Fig. 4). The dominance of this single large pore space, was found in all three peat samples, where it accounted for >99% of the active porosity (Table 3). The value of ϕ_A would therefore not significantly change if all but the single large pore were excluded from its calculation.

The dominance of a single pore is not unique to peat soil, and also occurs in mineral soils, and rock. For example, andesitic lava samples may contain large 3D pore clusters that account for >99% of the total porosity (Nakashima and Kamiya, 2007). However, peat soils are unique in the sense that the single large pore space dominates a total porosity which is approximately 2 to 3 times larger than that of mineral soils, and 4-times larger than that reported by Nakashima and Kamiya (2007) for rock. Therefore, for peat soils, a single large pore implies a more effective flowpath due to a greater degree of hydraulic connectivity among different soil regions, lower tortuosity of connected pores, and lower resistance to flow due to larger pore spaces.

Viewed in 2D (*e.g.* Fig. 4), the large void spaces separating the solid particles give the impression of an SLS (*i.e.* solid–liquid–solid) soil structure, as described by Gray et al. (1970), in that solid particles are not in direct contact with each other, but separated by liquid, and their position can change as the soil expands and contracts with changes in moisture content. By contrast, the solids of an SS (*i.e.* solid–solid) soil structure such as sands and silts, are in direct contact, and

Table 2
Summary of 2D image analyses of all 79 slices examined for each depth range measured at −40 cm soil water pressure: ϕ_A range is the maximum and minimum active porosities, $\bar{\phi}_A$ the average active porosity, $\bar{A}$ the mean pore area, and d_{cir} is the equivalent diameter of a circular pore of cross-sectional area $\bar{A}$.

Depth (cm)	ϕ_A range (%)	$\bar{\phi}_A$ (%)	$\bar{A}$ (mm^2)	d_{cir} (mm)	Largest pore (% of $\bar{\phi}_A$)	Density (cm^{-2})	p (mm^{-1})
0–6	57.7–60.0	58.6	1.59	1.42	1.24	36.7	1.29
6–12	58.2–60.2	58.9	1.77	1.50	1.17	33.2	1.83
12–18	46.1–49.7	47.9	0.71	0.95	0.91	67.9	1.89

Also reported is the percentage of $\bar{\phi}_A$ occupied by the largest pore, and the pore density, and the specific perimeter, p. The number of pores counted was 47,638, 43,065, and 88,005 for Upper, Middle and Lower samples respectively. The area of each 2D slice was 900×900 pixels, and the stack of 79 slices had a volume of 5.8 cm^3.

Table 3
Summary of 3D image analyses measured at −40 cm soil water pressure: ϕ_A is the active porosity, $\bar{V}$ is the mean pore volume, and d_{sph} is the equivalent diameter of a spherical pore of volume $\bar{V}$.

Depth (cm)	ϕ_A	$\bar{V}$ (mm^3)	d_{sph} (mm)	Largest pore (% of ϕ_A)	Density (cm^{-3})	s (mm^{-1})
0–6	58.6	0.49	0.98	99.87	1200	4.93
6–12	58.9	0.85	1.18	99.90	694	4.88
12–18	48.0	0.25	0.78	99.59	1934	5.14

Also reported is the percentage of ϕ_A occupied by the largest pore, and the pore density, and the specific surface area, s. The number of pores counted was 6998, 4044, and 11,278 for Upper, Middle and Lower samples respectively. The sample volume was 5.8 cm^3 (900×900×79 voxels).

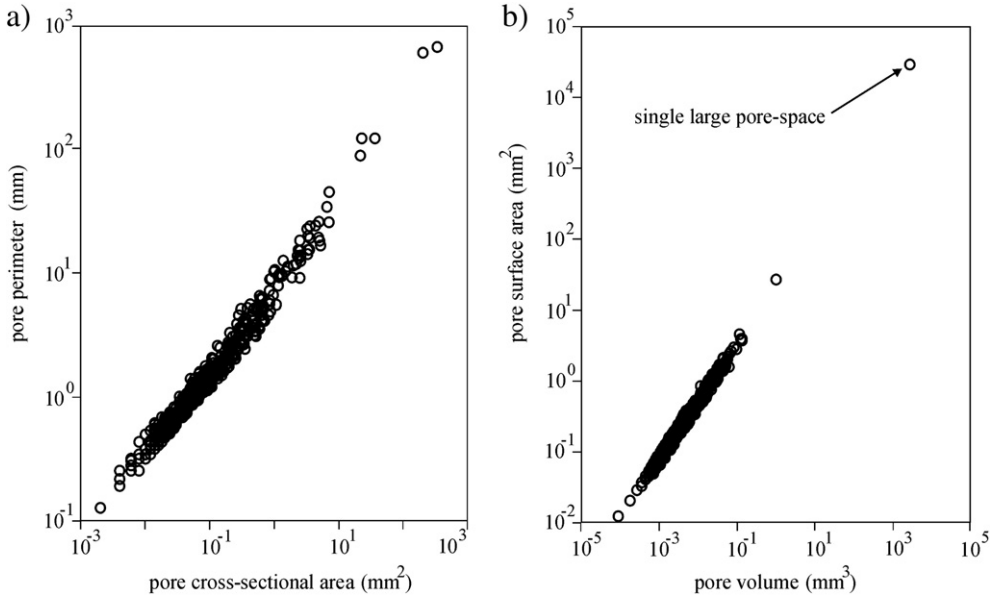

Fig. 3. Pore cross-sectional area plotted with pore perimeter for all pores in the single, upper-most 2D slice (900 × 900 voxels) of the Lower peat sample (a); and pore volume plotted with pore surface area from 3D analysis of Lower peat sample (b). The sample volume was 5.8 cm^3 (900 × 900 × 79 voxels).

are fixed in space regardless of the soil moisture content (Gray et al., 1970). An SLS-like structure distinguishes peat from other media in terms of the configuration of the liquid phase. Whereas SS soils hold water mainly at the points of contact in the form of wedges due to the capillary force; in SLS soils, most water lies within the adsorptive fields of the particle surfaces in the form of liquid films (Gray et al., 1970). A single, large pore in the context of an SLS-like soil structure therefore also implies a more effective continuous flowpath, since the occurrence narrow openings (*i.e.* necks) between discrete pores is reduced.

3.3. Deriving flow properties of peat from image analysis

Hydraulic conductivity is known to increase proportionately with the square of the mean pore diameter (Freeze and Cherry, 1979). However, porous media theory also recognise that the hydraulic conductivity is affected by the shape and orientation of pores, the total surface area of the solid–liquid interface and the tortuosity of flow-paths (Berryman and Blair, 1987). Recent studies have attempted to directly measure some of these properties. For example, Quinton et al. (2008) used the Kozeny–Carmen equation presented by Berryman

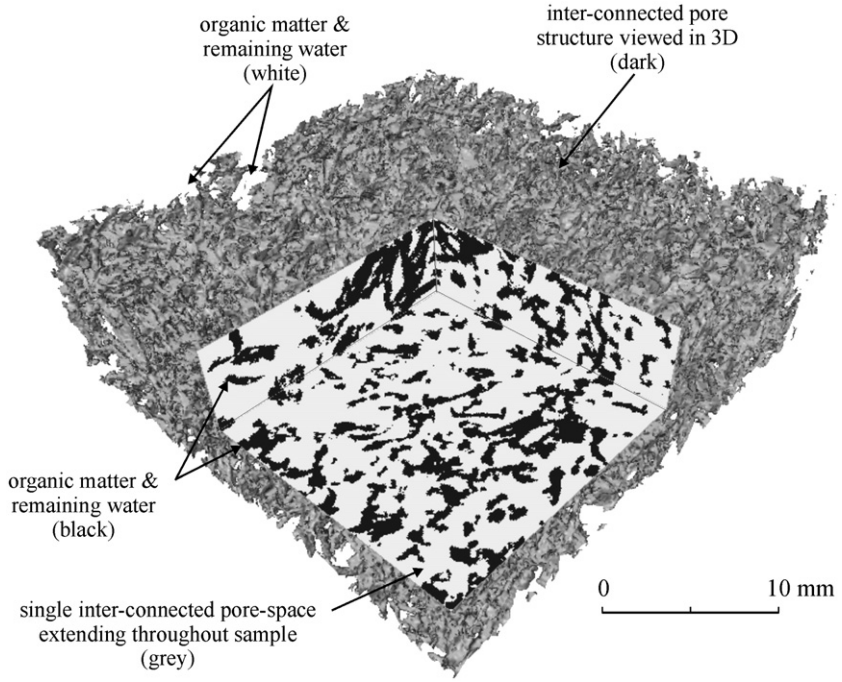

Fig. 4. 3D and binary 2D images of the Upper peat sample at −40 cm soil water pressure. Light areas represent the solid and liquid phases, and dark areas represent air-filled voids. The sample volume was 7.1 cm^3 (625 × 625 × 200 voxels) and was centred on the same point as the 5.8 cm^3 volume used for the measurement of peat properties.

and Blair (1987) to compute the hydraulic conductivity from pore geometry measurements on 2D images of peat. The Kozeny–Carmen expression includes a term for the specific surface area, s [L^{-1}] defined as the total surface area of pores per unit volume of porous media. It is often assumed that the specific surface area in three-dimensional porous media is approximately equal to the specific perimeter p [L^{-1}] in two-dimensional cross-sections (Bear, 1972), defined as the total perimeter of pores per unit cross-sectional area;

$$p = \sum_i P_i / A_{\text{img}}, \tag{6}$$

where P_i [L] is the perimeter of the i-th pore in the image and A_{img} [L^2] is the total image area. Quinton et al. (2008) demonstrated that the large decrease in saturated horizontal hydraulic conductivity of peat with depth was due to compaction-induced anisotropy of the peat profile. That is, compaction of pores reduces their 2D hydraulic radius (*i.e.* cross-sectional area/perimeter), which therefore increases their hydraulic resistance. In the present study, the specific perimeter increased with depth (Table 2), indicating increased resistance to flow with increasingly decomposed (*i.e.* deeper) peat. The values of p reported in Table 2 are also within the range of the 14 values measured by Quinton et al. (2008) for a wider range of peat depths ($p = 0.96$ to 6.79).

In 3D, the specific perimeter is replaced by the specific surface (s), calculated as

$$s = \sum_i S_i / V_{\text{img}}, \tag{7}$$

where S_i is the surface area of the i-th pore and V_{img} is the total image volume. The specific surface was found to be larger than the specific perimeter p by a factor of 2.56 (upper sample) to 2.71 (lower sample). These ratios were relatively large compared to that of 1.27 computed for each layer, assuming the relation: $s = 4p/\pi$ of Doltsinis and Dattke (2001). However, that relation assumes a relatively simple medium of spherical pores, and is therefore unlikely to apply to complex, anisotropic media such as peat. Peat fibres are often preferentially oriented in the horizontal direction due to the weight of overlying sediments. As a result, the active porosity may also be preferentially orientated in the same direction. Because vertical compaction increases with depth below the ground surface, so too does the horizontal elongation of pores, which would lead to increased anisotropy with depth, and this may be suggested by the increasing s:p ratios with depth (Table 3). The value of s is known to depend on the soil porosity (du Plessis, 2007); however, the present study demonstrates that ϕ_A has essentially the same value when measured in 2D or 3D, and therefore the porosity cannot explain the relatively large s:p ratios reported here. However, s is also known to be influenced by the number, shape, size, and length of pores and their distribution (Salem and Chilingarian, 1999). In addition, the values of s and p in the present study would be affected by the geometric properties of the interface between the liquid films and air-filled spaces, as that was the only surface that could be defined.

Relating media properties to hydraulic conductivity is more complicated when considering unsaturated peat, since the measured values of such properties varies with moisture content, due to volume changes of the peat (*e.g.* Table 1), and to the redistribution of the liquid phase. For example, the latter directly affects the tortuosity of flow, and therefore the unsaturated hydraulic conductivity. By comparing the 3D images of successive scans from the upper sample core, the flow network is elucidated for the 7.1 cm^3 sub-sample by identifying the group of non-void voxels that become void voxels following the incremental decrease in soil water pressure. Defined in this way, the flow network is not simply the total moisture within the active porosity, since not all of that water drains in response to a given range of soil water pressure. The flow network depicted in Fig. 5 occupies a unique 3D space within the peat sample for each pressure range, and represents the outer layers of water films.

The white spaces within Fig. 5 may include moisture films that were not well-connected to active flowpaths and therefore did not drain under the applied pressure. By contrast a high density of dark space implies well-connected water films that therefore drained readily. There appeared to be greater drainage from the edges than the centre of the sample volume in the −18 to −30 cm pressure range (Fig. 5c); while the flow network appears more evenly distributed throughout the sample for the other three pressure ranges. The incremental decrease in the flow network volume with decreasing pressure depicted in Fig. 5 appears to have occurred by the thinning and disaggregation of moisture films throughout the sample, rather than by preferential drainage of specific regions.

The flow network diminished from 17.6% of the sample volume in the first increment (Fig. 5a) to 9.0% in the final increment (Fig. 5d). Considering that for these two values, the associated volumetric moisture content of the upper sample measured from CT images (Fig. 2) was 0.65 and 0.42 respectively, the moisture content of the flow network remained approximately one-quarter that of the total volumetric moisture content as the sample drained. The sum of the four flow network volumes presented in Fig. 5 indicates that ~52% of the 7.1 cm^3 sample volume became air-filled by the end of the experiment. However, the measured reduction in volumetric moisture of 23% (*i.e.* 0.65–0.42) by gravimetric means, indicates that only about half of the water that was evacuated from voxels also drained from the sample volume. The remaining water would have been redistributed within the volume, such as into previously air-filled voxels along flowpaths.

4. Conclusions

This study found that X-ray tomography is an effective means of measuring physical and hydraulic properties of peat. The relatively small average solid fraction (<10%) introduced only a small, systematic error when combining the liquid and solid fractions into the single class of non-void voxels. Measurement of the solid fraction is easily done and necessary to correct CT-based estimates of volumetric moisture content. The 2D and 3D measurements produced very similar values of active porosity, indicating that 2D images can be used to accurately estimate the fraction of inter-particle space within the 3D media.

Image analysis at the −40 cm pressure level indicated that on average, the active porosity of the peat samples was ~0.6; while gravimetric analysis indicated a solid fraction of ~0.1. Given the inactive porosity of ~0.2 (Quinton et al., 2008), these measurements suggest that ~0.1 remained in water films at −40 cm pressure. The latter should be added to the value of the active porosity since water films occupy the inter-particle space. This amount of water still present in films at −40 cm pressure seems reasonable, since the water retention characteristic curves derived by Quinton and Hayashi (2007) on peat samples from the upper peat layer (i.e. upper 20 cm of peat) from Scotty Creek indicate a volumetric moisture content of ~0.35 associated with −40 cm soil water pressure; and the residual of 0.2 was not reached until soil pressure was below −100 cm. The true active porosity, measured when the inter-particle space is free of water, should therefore approach 0.7.

This study also found that 2D and 3D analyses of the same peat sample provide some contrasting results. For instance, the specific perimeter measured in 2D was smaller than the specific surface area measured in 3D, despite the common assumption that they are approximately equal. The 2D and 3D analyses also produced different results with respect to the distribution of pore sizes. The 2D analysis suggests a relatively gradual transition from small to large pores, with the largest pore representing <2% of the active porosity. However, the 3D analysis indicates a single, large pore space representing >99% of the active porosity. The 3D view of the peat therefore suggests that the active porosity can be treated as a single, large pore space

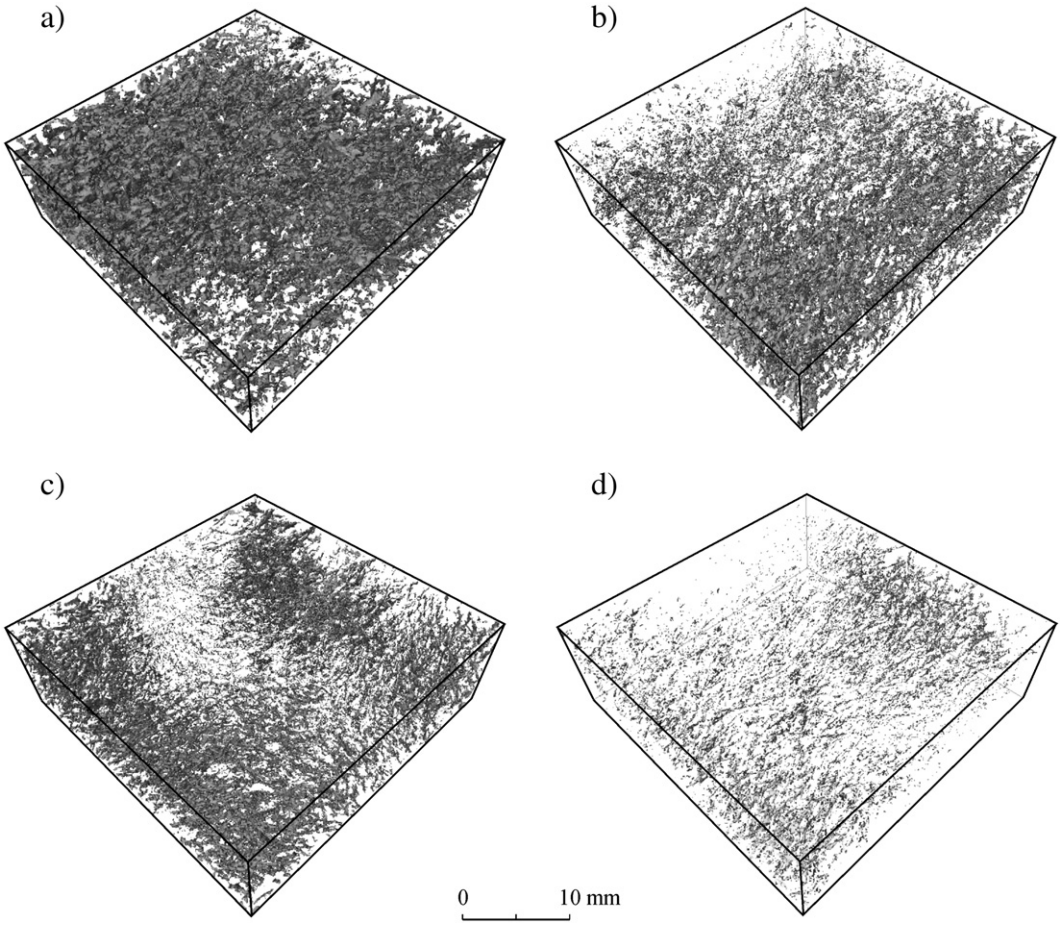

Fig. 5. The flow network defined by the region of ϕ_A that had drained as the soil water pressure decreased from −2 to −10 cm (a), −10 to −18 cm (b), −18 to −30 cm (c), and −30 to −40 cm (d). The volume of the flow network expressed as a percentage of the sample volume was 17.6% (a), 11.8% (b), 14.1% (c) and 9.0% (d). The sample volume was 7.1 cm^3 (625 × 625 × 200 voxels) and was centred on the same point as the 5.8 cm^3 volume used for the measurement of peat properties. This analysis was conducted on the Upper peat sample.

with a complex configuration; in contrast to the 2D view of the peat matrix as an assemblage of discrete pores of variable size. A single, large pore in the context of an open (i.e. SLS-like) soil structure implies an effective, continuous flowpath for soil drainage, since the occurrence of narrow openings (*e.g.* necks in mineral soils) between discrete pores is reduced.

The active porosity can therefore be viewed as a single, large pore space, within which lies the flow network. The volume and configuration of the flow network was elucidated for discrete ranges of soil water pressure that typically occur in the field. The flow network diminished from 17.6% to 9.0% of a sample volume as the volumetric moisture content lowered from 0.65 to 0.42. This volume loss occurred by the thinning and disaggregation of moisture films, while the flow network maintained a relatively even spatial distribution. Comparison of the fraction of voxels that were evacuated of water, with the reduction in volumetric moisture content suggests that about half of the water in the flow network drained from the sample, while the rest was redistributed, but remained within the volume.

Acknowledgements

The authors wish to thank Mr. J. Wright and Mr. R. Pilling of the Water Survey of Canada (Fort Simpson, NWT) for their generous logistical support in the field. We also wish to thank Dr. D. Elrick, University of Guelph, for his help with designing the soil water pressure apparatus, and his valued insights and those of Dr. M. Hayashi, University of Calgary at various stages of this research. Mr. P. Whittington's assistance in the field with obtaining peat samples, and in the laboratory is gratefully acknowledged. Mr. Trevor Myers is thanked for conducting the CT scans. We also acknowledge the support of the Natural Sciences Engineering and Research Council, and the Canadian Foundation for Climate and Atmospheric Sciences.

References

Berryman, J.G., Blair, S.C., 1987. Kozeny–Carman relations and image processing methods for estimating Darcy's constant. Journal of Applied Physics 63, 2221–2228.
Bear, J., 1972. Dynamics of Fluids in Porous Media. Dover Publications, New York. 764 pp.
Boelter, D.H., 1976. Methods for analysing the hydrological characteristics of organic soils in marsh-ridden areas. Hydrology of Marsh-Ridden Areas. Proceedings of IASH Symposium Minsk., 1972. IASH, UNESCO, Paris, pp. 161–169.
Boelter, D.H., Verry, E.S., 1977. Peatland and water in the northern lake states. General Technical Report NC-31. U.S. Dept. of Agriculture, Forest Service, North Central Forest Experiment Station, St. Paul, MN.
Carrier, W.D., 2003. Goodbye, Hazen; Hello, Kozeny–Carman. Journal of Geotechnical and Geoenvironmental Engineering 129 (11), 1054–1056.
Doltsinis, I., Dattke, R., 2001. Modelling the damage of porous ceramics under internal pressure. Computer methods in applied mechanics and engineering 191, 29–46.
du Plessis, M., 2007. Relationship between specific surface area and pore dimension of high porosity nanoporous silicon — model and experiment. Physica Status Solidi 204 (7), 2319—2328.
Elliot, T.R., Heck, R.J., 2007. A comparison between 2D vs 3D thresholding of X-ray CT imagery. Canadian Journal of Soil Science 84 (4), 405–412.
FitzPatrick, E.A., 1984. Soil Micromorphology. Chapman and Hall, London, UK.
Freeze, R.A., Cherry, J.A., 1979. Groundwater. Prentice-Hall, Englewood Cliffs, NJ. 604 pp.
Gray, D.M., Norum, D.I., Wigham, J.M., 1970. Infiltration and physics of flow of water through porous media. In: Gray, D.M. (Ed.), Handbook on the Principles of Hydrology. Canadian National Committee of the International Hydrological Decade, Ottawa.
Hazen, A., 1911. Discussion of "Dams on sand formations," by A.C. Koenig. Transactions of the American Society of Civil Engineers 73, 199–203.

Hoag, R.S., Price, J.S., 1997. The effects of matrix diffusion on solute transport and retardation in undisturbed peat in laboratory columns. Journal of Contaminant Hydrology 28, 193–205.
Hayward, Clymo, 1982. Profiles of water content and pore size in Sphagnum and peat and their relation to peat bog ecology. Proceedings of the Royal Society London B 299–325.
Ingram, H.A.P., 1978. Soil layers in mires: function and terminology. Journal of Soil Science 29, 224–227.
Nakashima, Y., Kamiya, S., 2007. Mathematica programs for the analysis of three-dimensional pore connectivity and anisotropic tortuosity of porous rocks using X-ray computed tomography image data. Journal of Nuclear Science and Technology 44 (9), 1233–1247.
National Wetlands Working Group (NWWG), 1988. In: Tarnocai, C. (Ed.), Wetlands of Canada: Ecological Land Classification Series, vol. 24. Sustainable Development Branch, Environment Canada, Ottawa, Ontario, and Polyscience Publications Inc., Montreal, Quebec. 452 pp.
Olsen, P.A., Borresen, T., 1997. Measuring difference in soil properties in soils with different cultivaion practices using computer tomography. Soil & Tillage Research 44, 1–12.
Quinton, W.L., Hayashi, M., 2007. Recent advances toward physically-based runoff modeling of the wetland-dominated, Central Mackenzie River Basin. Cold region atmospheric and hydrologic studies. In: Woo, M.-K. (Ed.), The Mackenzie GEWEX Experience : Hydrological Processes, vol. 2. Springer, pp. 257–279.
Quinton, W.L., Gray, D.M., Marsh, P., 2000. Subsurface drainage from a hummock-covered hillslope in the Arctic tundra. Journal of Hydrology 237, 113–125.
Quinton, W.L., Hayashi, M., Carey, S.K., 2008. Peat hydraulic conductivity in cold regions and its relation to pore size and geometry. Hydrological Processes 22, 2829–2837.
Rasband, W.S., 2007. Image J, U. S. National Institutes of Health, Bethesda, Maryland, USA, http://rsb.info.nih.gov/ij/, 1997–2007.
Salem, H.S., Chilingarian, G.V., 1999. Determination of specific surface area and mean grain size from well-log data and their influence on the physical behavior of offshore reservoirs. Journal of Petroleum Science and Engineering 22, 241–252.